Journal of Naval Architecture and Marine Engineering
December, 2021
http://dx.doi.org/10.3329/jname.v18i2.52134 *http://www.banglajol.info*

HYDRODYNAMIC PERFORMANCES OF A WALL TYPE BREAKWATER - A PHYSICAL AND NUMERICAL APPROACH

V. Kumaran [1*], Manu[1], Subba Rao[1] and I. Srinivasula Reddy[2]

[1]Department of Water Resources and Ocean Engineering, National Institute of Technology Karnataka, Surathkal, Mangalore 575025, India, *Email: vkumaranms@gmail.com, manunitk77@gamil.com, surakrec@gmail.com

[2]Department of Civil Engineering, KSRM College of Engineering, Kadapa-516003, India, Email: reddysrinu@ksrmce.ac.in

Abstract:

This paper investigates hydrodynamic performances of a wall-type breakwater through a physical model approach and validated using a numerical model based on the Volume of Fluid (VOF) method. The investigations are carried out for varying wave characteristics with the depth of water, 0.50 m. A 2D numerical wave flume is developed using ANSYS- Fluent platform by considering the VOF method and incompressible open channel fluid flow. The wave boundary conditions are adopted by solving the Reynolds-Averaged Navier Stokes equations (RANS equation) especially with the k—ε model to examine the effects of turbulence on the numerical results. The hydraulic performance characteristics on the wall-type breakwater are analyzed for different wave characteristics. It is found that results obtained from the numerical investigations are in good agreement with the experimental ones.

Keywords: Ansys-Fluent; Caisson type breakwater; VOF method; wave interaction; RANS equation

NOMENCLATURE

d	Still Water Depth	WCSPH	Weakly Compressible Smoothed Particle
H_i	Incident Wave Height	RANS	Reynolds Averaged Navier – Stokes Equation
Ho	Deepwater Wave Height	T	Wave Period
CB	Caisson Breakwater	L	Wave Length
VOF	Volume of Fluid	Re	Reynolds Number
OWC	Oscillating Water Column	P	Wave Force
CFD	Computation Fluid Dynamics	d/L	Relative Water Depth
FDM	Finite Differences Method	H_i/L	Wave Steepness
UDF	User Defined Function		

1. Introduction

The structural interaction of ocean waves is a common phenomenon for free-surface fluid flow hydrodynamics in coastal engineering. Understanding the fundamental physical properties and analytical computations is imperative to assess the various loads on coastal structures and their responses. Experimental studies on ocean wave structure interaction require well-sophisticated laboratory facilities and wave response measuring systems. The experimental studies on ocean wave structure interaction are time-consuming and expensive. The rapid development in modern computational methods resulted in CFD-based simulation of ocean wave structure interaction getting more popular. Many researchers are working on CFD-based simulations to study ocean wave hydrodynamics, sediment transport, ocean wave energy, etc., due to less time consumption, economical, and accuracy of results when compared to the experimental methods. In the recent past, many researchers (Xie et al. 1981, Gao et al., 1997, Kasem et al.2011) have developed CFD models to simulate the ocean waves, which are non-linear and unsteady in their behavior. Gao et al. (1998) studied the clapotis interaction for broken waves along with vertical breakwater and classified their wave motions (standing wave, breaking clapotis, and broken clapotis). The authors concluded that broken clapotis is a more severe wave motion than the other two wave motions. Xie et al. (1981) worked on experimental studies on the interaction of the clapotis wave with a vertical breakwater

1813-8535 (Print), 2070-8998 (Online) Received on: February 2021

and simultaneously measured the maximum horizontal orbital velocity distributions for non-breaking wave conditions. Researchers (Vijay et al. 2019; Venkateswarlu et al. 2020) studied the different vertical barriers with varying porosity levels to analyze the hydraulic properties using the potential flow theory and the boundary element method. Kumaran et al. (2021) investigated the performances of wall type breakwater and its toe stability for non-breaking wave conditions. Hajivalie et al. (2009) concentrated on numerical simulation of the interaction of a broken wave with a vertical breakwater using the RANS equation. Kasem et al. (2010) investigated the numerical multiphase model to study the wave generation for multiple submerged breakwaters. In their model, the level set method was used to track the free surface elevation (η) and complex features near the various submerged structures. Yong-xue Wang et al. (2011) developed a 3-D numerical model to simulate ocean wave structure interaction on perforated quasi-ellipse caisson using FDM and VOF methods and validated the results obtained from the numerical model using experimental results for better performance. Qingjie et al. (2011) studied the simple numerical generation of ocean waves. They compared the water surface elevation (η) values obtained from the numerical method with theoretical approaches, optimizing the wave energy converters. Sonia Ben Hamza et al. (2015) investigated the dynamic flow field in and around an obstacle due to the non-linear effects, provides the wave simulation interaction with vortex structures of various shapes. D.Ning et al. (2016) analyzed the hydrodynamic characteristics of submerged breakwaters using both experimental and numerical methods. The authors considered the fully non-linear and 2-D Boundary Element Method to develop a numerical model and validated the numerical model using a series of experimental results.

Bakhtiary et al. (2017) developed Weakly Compressible Smoothed Particle Hydrodynamics (WCSPH) using the 2-D Lagrangian model to simulate the hydrodynamic process during impinges of clapotis waves on a Caisson breakwater. Lin Zhao et al. (2019) investigated the numerical simulation of regular wave interaction with perforated caisson breakwater. The authors used FLOW -3D software to develop three-dimensional finite-difference models. Scarpetta et al. (2017) numerically simulated a full-scale U-shaped duct Oscillating Water Column (U-OWC) breakwater based on the CFD approach. Two-dimensional unsteady CFD simulation is carried out by solving the RANS equations, and the VOF model was used to account for the water-air interaction. The CFD model allowed for a detailed analysis of the interaction between a U-OWC device and incident waves. Somervell et al. (2017) investigated the hydrodynamic characteristics of a vertical cellular breakwater with varying different porosities of the upper and lower parts of the test model. The eigenfunction expansion analytical method was used to study the hydrodynamic performance of the cellular breakwater.

In the present work, numerical simulations are investigated for the 2D wave flume along with a wall-type breakwater. Some of the critical phenomena associated with the wall type breakwater, such as wave forces, wave reflection, and wave run-up, are revealed by the numerical analysis and also performed for comparison with experimental laboratory results. This constitutes the primary purpose of this study. This paper is organized as follows: Section 2 details the experimental setup and configuration of the test model in the Wave Mechanics Laboratory, National Institute of Technology Karnataka (NITK); Section 3 elaborates the mathematical background; Section 4 discusses the boundary conditions and input parameters related to the numerical study; Section 5 discusses the various results of the experimental and numerical approach.

2. Experimental Setup

The physical model studies are carried out in 2D-wave flume available in wave mechanics Laboratory, National Institute of Technology Karnataka (NITK). The experimental setup consists of a bottom-hinged paddle-type wave maker that can produce regular monochromatic waves. The generated waves by wave paddle pass through thin asbestos vertical sheets to form smooth waves without turbulence. The wave flume has active wave absorption for absorbing the reflecting wave from the test model. The wave flume is 50 m long and 0.72 m wide, and 1.1 m high. The wave generator is operated by an induction motor of capacity 7.5 HP, 11 kW, and 1450 rpm. An inverter device regulated the induction motor with a frequency range of 0-50 Hz, which rotates the motor at 0-155 rpm. The wavemaker can generate regular monochromatic waves of height ranging from 0.06 m to 0.2 m and wave periods ranging from 1 s – 3 s at a maximum water depth of 0.7 m. The wave flume calibration is performed without the test model to measure incident wave heights – wave periods.

The wall-type breakwater test model is constructed using concrete, and the model is cast with dimensions of 0.7 m width, 0.9 m height, and 0.5 m depth having a wall thickness of 50 mm. The model is placed in a wave flume on a 30 mm thick aggregate bed and supported by its dead weight. (Kumaran et al. (2020). In the study, all the

experiments are conducted at a water depth of 0.5 m. Experiments are conducted at different combinations of wave heights (0.12 m, 0.14 m, 0.16 m, and 0.18 m) and different wave periods (2.2 s, 2.4 s, 2.6 s, 2.8 s). The normalized hydrodynamic parameters related to the present study are relative water height (Hi/d, ranging from 0.24 to 0.36), relative water depth (d/L, ranging from 0.11 to 0.084), and incident wave steepness (Hi/L, ranging from 0.02 to 0.04). Figure 1. Illustrated the experimental setup for the present study.

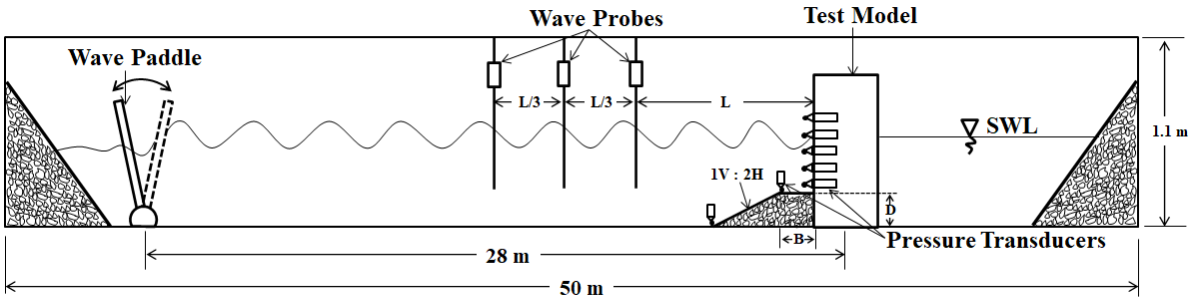

Figure 1: Experimental setup

The incident surface elevations of the waves during experiments are measured using wave probes placed at the seaside of the model. The wave force on the wall-type breakwater is measured by placing pressure transducer at selective locations on the test model. The schematic picture of planned wave probe locations and a picture of the actual model with a pressure transducer is given in Figure 2 (a) and Figure 2 (b). The pressure transducer measures the pressure on a particular point of the model at each instant of time. During the experiment, the surface elevations data measured by wave probes and pressure data at selected locations of the model are acquired by the data acquisition system. The data is used to calculate the maximum total pressure acting on the model during each set of experiments. The measured surface elevation data and calculated total pressure on the vertical caisson breakwater model are used to validate the same obtained from the numerical simulations.

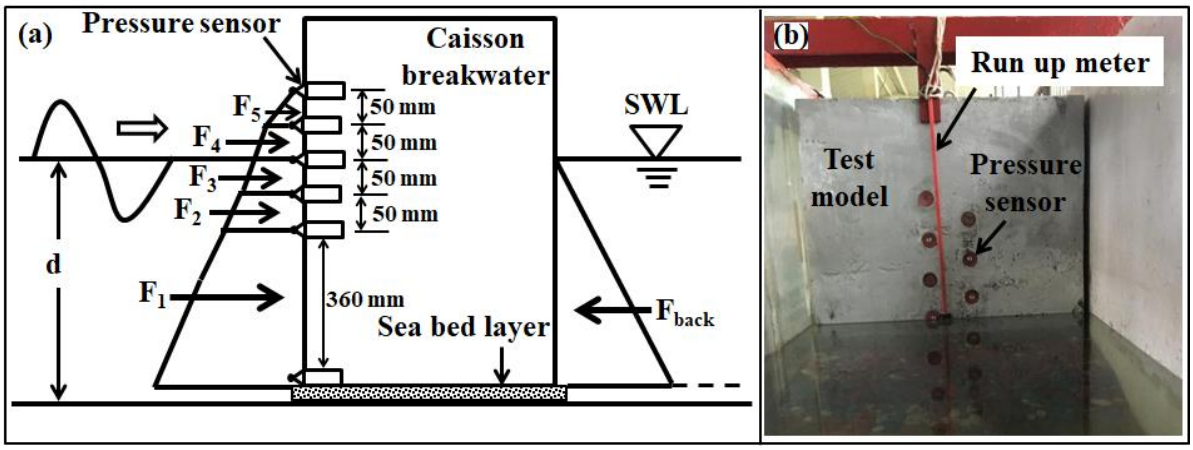

Figure 2. (a): Schematic pressure sensor locations and (b) photographic view of pressure sensors and run-up meter on the test model.

3. Mathematical Background

The two-dimensional numerical model is developed using the Volume of Fluid (VOF) formulation in FLUENT in the present study. Navier-Stokes equation (Eq. 1) and continuity equation (Eq. 3) are used to formulate the wave's non-linear and free surface flow motion. The water is assumed to be incompressible, Newtonian fluid, and the density of water does not change with time.

$$\rho\left(\frac{\partial w}{\partial t}+w\nabla w\right)=-\nabla p+\nabla\mu\left(\nabla w\right)+F \tag{1}$$

In two dimensional Cartesian coordinate system, the equation (1) can be rewritten as,

$$\rho\left(\frac{\partial u}{\partial t}+u\frac{\partial u}{\partial x}+v\frac{\partial u}{\partial y}\right)=-\frac{\partial p}{\partial x}+\mu\left(\frac{\partial^2 u}{\partial x^2}+\frac{\partial^2 u}{\partial y^2}\right)+\rho g_x \tag{2a}$$

$$\rho\left(\frac{\partial v}{\partial t}+u\frac{\partial v}{\partial x}+v\frac{\partial v}{\partial y}\right)=-\frac{\partial p}{\partial y}+\mu\left(\frac{\partial^2 v}{\partial x^2}+\frac{\partial^2 v}{\partial y^2}\right)+\rho g_y \tag{2b}$$

Where w is the fluid velocity; u & v are velocity components in x & y-direction; p is the fluid pressure; ρ is the fluid density; μ is the dynamic fluid viscosity. In equation (1), the first term corresponds to the inertial forces; the second term corresponds to pressure/forces; the third term corresponds to viscous forces; the fourth term corresponds to external forces applied to the fluid. Equations 2a and 2b represent the Navier-Stokes equation in a 2D Cartesian coordinate system. The continuity equation in conservation form is in equation (3).

$$\frac{\partial u}{\partial x}+\frac{\partial u}{\partial y}=0 \tag{3}$$

Boundary conditions: In FLUENT, the Volume of Fluid (VOF) scheme satisfies kinematic free-surface boundary condition (Eq. 4) and dynamic free surface boundary condition (Eq. 5), the no Flux - Normal boundary condition (Eq. 6) satisfies by using wall condition. Where P_0 is pressure on the free surface (η); η is free surface elevation; ϕ is velocity potential.

$$\frac{\partial \eta}{\partial t}=-\nabla\varnothing\nabla\eta+\frac{\partial\varnothing}{\partial y} \tag{4}$$

$$\frac{\partial\varnothing}{\partial t}=-g\eta-\frac{1}{2}\left|\nabla\varnothing\right|^2-\frac{p_0}{\rho} \tag{5}$$

$$\frac{\partial\varnothing}{\partial\eta}=0 \tag{6}$$

4. Numerical Model

A two-dimensional numerical wave flume is modelled with dimensions of length 16 m, the height of 1.1 m. The water depth of 0.5 m and test model height of 0.9 m are considered for the present numerical investigation. The schematic of the numerical flume model and its dimensions are given in Figure 3. The test model is located at a distance of 14 m from the wave generation zone. To obtain the surface elevation at required positions (at a distance of L, L+(L/3), and L+(2L/3) from the test model) even at maximum wavelength conditions (6 m), 14 m distance is maintained between the test model and wave generation point. The obtained data are used to calculate the wave reflection coefficient (Kr). Initially, the hydrostatic conditions (water at rest) of the flume, the generation of wave process is initiated by assigning a regular wave motion in the wave flume using a user-defined function with the movement of the flap-type paddle. The governing equations (conservation of mass and moment) are solved by making the computational space into a finite number of a control volume. As an initial condition, static pressure is given for the liquid face, and the volume of the fluid model is used to generate the free surface between air and water medium. The test model and the flume walls are assigned as No-slip wall boundaries. The upper domain boundary and the right-side wall of the flume model are defined as pressure outlets. Zero-gauge pressure is determined at the upper domain boundary by considering the atmospheric pressure as the reference pressure.

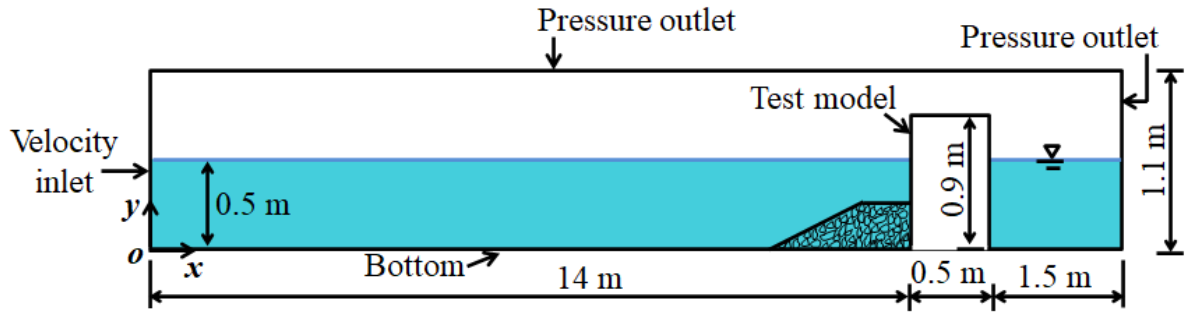

Figure 3: Geometry of the flume model with boundary conditions.

The inappropriate selection of mesh can affect the accuracy of simulation results, computational efficiency, and solution stability. The proper wave formation can be obtained when the model is developed with a minimum of 200 grids per wavelength (Arun Kamath 2012), and the aspect ratio (ratio of higher dimension to lower dimension of element) of an element should be less than 10 (Marques Machado et al. 2018). In the present study, to generate waves at a maximum wavelength of 6 m conditions maximum element length of 0.03 m is required. So all the experiments are simulated with a mesh size of 0.02 m and at an element aspect ratio of one.

Figure 4 illustrates the two-dimensional free mesh used nearer the test model. The total number of nodes and elements used are 40676 and 40002. The quality of results also depends on time discretization and the type of transient formulation used for the study. Implicit schemes are more stable than explicit schemes, even at lower time step sizes. Hence, the second-order implicit method with a time step of 0.01 seconds is used in this study. Marques Machado et al. (2018) concluded the time step of a maximum 1/200th of the corresponding wave period was the optimum time step size for numerical modeling. All the experiments are simulated for up to 15 seconds to get the proper reflected wave data to calculate the reflection coefficient.

The transient gravity-based model is chosen for the present study. VOF model with open channel wave boundary conditions is adopted, and the implicit formulation is used for the volume fraction parameter. The simulations are modeled with two-phase incompressible fluids (air and water) having a constant density of 998 kg/m3 for water and a constant density of 1.225 kg/m^3 for air. K-epsilon viscous models are more suitable for turbulent open-channel flows (Sunny Kumar Poguluri 2020). In this study, the standard k-epsilon viscous model is used for wave generation. The selection of wave boundary conditions and wave theory depends on wave steepness and relative water depth. Recommended code practice DNV RP C 205 (2010) explained the suitable wave theories for various wave conditions (shallow to deep water). Shallow/intermediate wave boundary condition is applied at the velocity inlet, and Stokes's third-order wave theory is used for all the Numerical simulations.

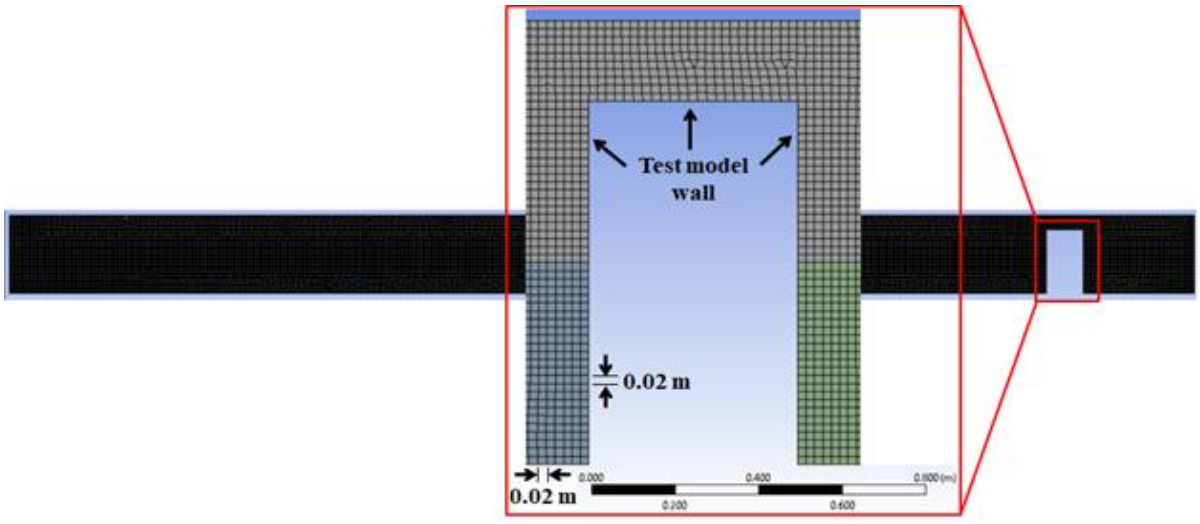

Figure 4: Fluent mesh model closer to the test model.

4.1 Mesh independence study

Figure 5 shows the variation for different grid sizes with reflection coefficient (K_r) for the area of interest (test model). The quality of results also depends on time discretization and the type of transient formulation used for the study. The different grid sizes considered for the present study are 0.1 m, 0.04 m, 0.02 m, and 0.01 mm. The convergence of the solution independent of mesh is obtained for 0.02 m and 0.01m grid sizes and the corresponding solutions are compared with experimental values. The grid size of 0.02 m is considered for the present study owing to the fact that it takes less computational time on account of a smaller number of elements.

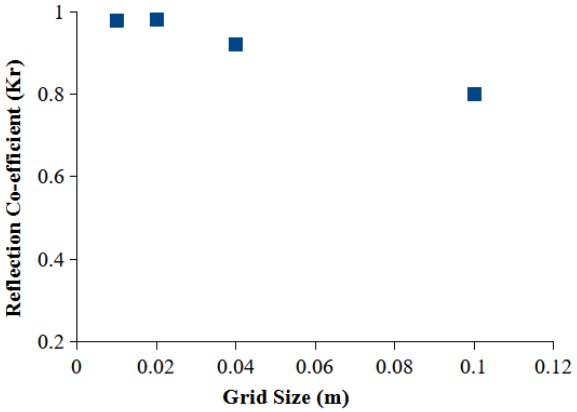

Figure 5: Mesh Independence.

Table 1 illustrates the statistical comparison of Fluent output with experimental results. Root mean square error (RMSE) is used as an index of comparison. The RMSE formula is given in Equation (8). The statistical results obtained at different wave heights (0.12 m and 0.18 m) and different wave periods (2.2 s and 2.8 s) are introduced in Table 1. The statistical results show that Fluent outputs have less deviated from experimental results.

$$\text{RMSE} = \sqrt{\frac{1}{N}\sum_{i=1}^{N}(y_{Numerical} - y_{Experimental})^2} \quad (1)$$

Table 1: Statistical comparison of Fluent and Experiments

Experimental parameters	RMSE
H_i = 0.12 m, T = 2.2 s	0.0210
H_i = 0.12 m, T = 2.8 s	0.0341
H_i = 0.18 m, T = 2.2 s	0.0258
H_i = 0.18 m, T = 2.8 s	0.0198

5. Results and Discussions

Numerical analysis is carried out to find the wave force, reflection coefficient, and run-up on a wall-type breakwater. The results obtained from numerical computations are validated using the experimental findings. The numerical simulations are performed at different wave periods (2.2 s, 2.4 s, 2.6 s & 2.8 s) and different wave heights (0.12 m, 0.14 m, 0.16 m & 0.18 m) at a water depth of 0.5 m.

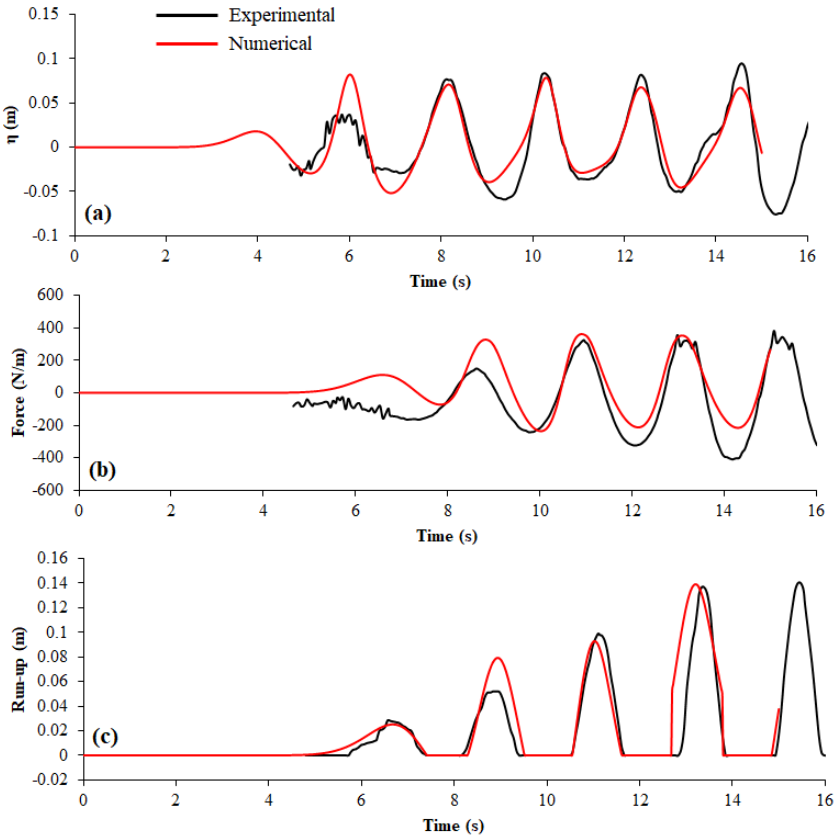

Figure 6: Comparison of experimental and numerical (a) surface elevation, (b) force on a vertical caisson, and (c) run-up for wave height 0.12 m and wave period 2.2 s condition.

The surface elevations at a distance of L, L+(L/3) & L+(2L/3) from vertical caisson are measured during each set of experiments. The same data is used to validate the surface elevation data at respective positions computed from numerical analysis. Figure 6 (a) and Figure 7 (a) shows a comparison of both numerical and experimental surface elevation data at L+(L/3) distance from the test model. Experimentally, the wave force on the test model at each instant of time is calculated from the measured wave pressure data at each moment at selected locations on the test model, as shown in Figure 1 (a). During experimentation, the wave forces on the test model are measured in the x-direction. Hence in the numerical analysis, the sum of forces in x-direction on test model walls (Figure 4) at an instant of time is considered as a force on the test model at that particular instant of time. Figure 6 (b) and Figure 7 (b) shows the comparison of force on wall breakwater over a time obtained from experimental and numerical results. The run-up is measured using a capacitance-based run-up meter placed on the front face of the test model shown in (Figure 1 (b)). In the numerical analysis, the length of water volume fraction on the sea sidewall (front face) of the test model is considered for the run-up analysis Figure 6 (c) and Figure 7 (c) shows the temporal variations of run-up obtained from experiments and numerical analysis. Figure 6 and Figure 7 show that the computed numerical surface elevations, wave force, and run-up results showed good agreement with experimental findings.

Unstable wave formation is observed from both experimental and numerical results at 0.18 m wave height and 2.8 s wave period test condition due to a higher Ursell number. In the VOF model, two phases (air & water) are not interpenetrating, and the fraction of the volume of a phase in a particular cell is calculated as a fraction of volume.

The two phases (air and water) flow fields are assumed to be unsteady and solved by the Navier-Stokes and the (RANS) equations. The wave propagation and interaction of the wave with the test model shown in Figure 8 represent the water volume fraction in a numerical wave tank during waves' progress. Figure 6 (b) shows that the wall breakwater experienced the initial wave force at 6 s, maximum force at 11.1 s, and minimum force at 12.2 s.

The water volume fraction graph (Figure 8) is the numerical evidence for forces acting on wall breakwater at different instants of time. Figure 8 is also evidence for run-up at the different instants of time shown in Fig 6 (c).

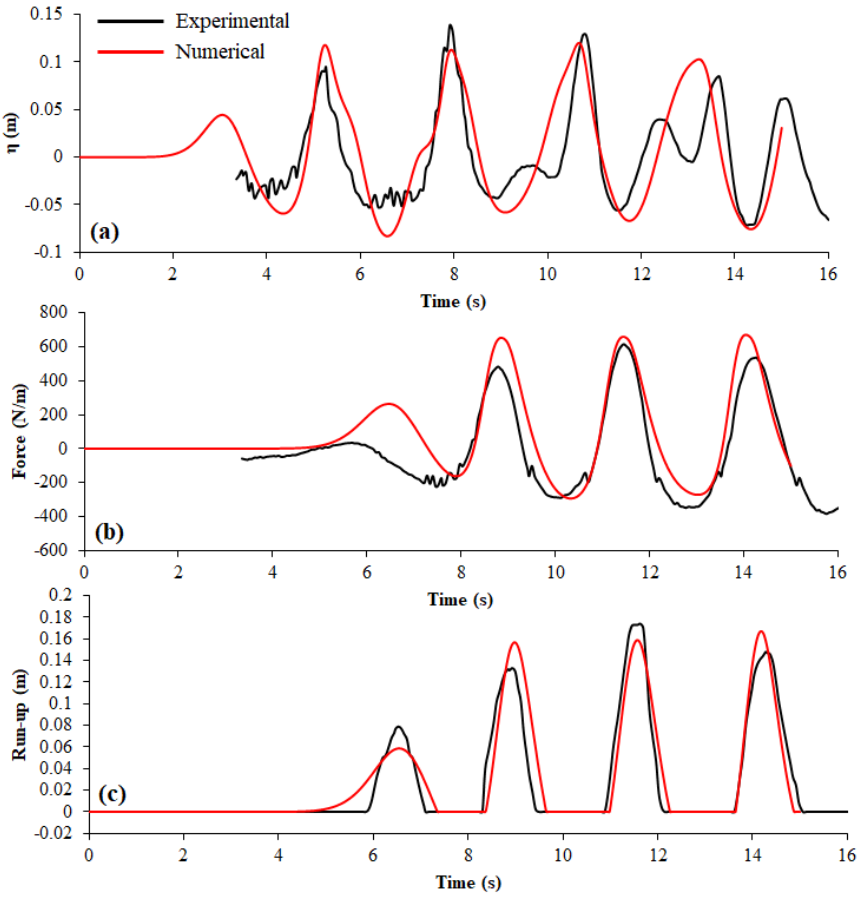

Figure 7: Comparison of experimental and numerical (a) surface elevation, (b) force on a vertical caisson, and (c) run-up for wave height 0.18 m and wave period 2.8 s condition.

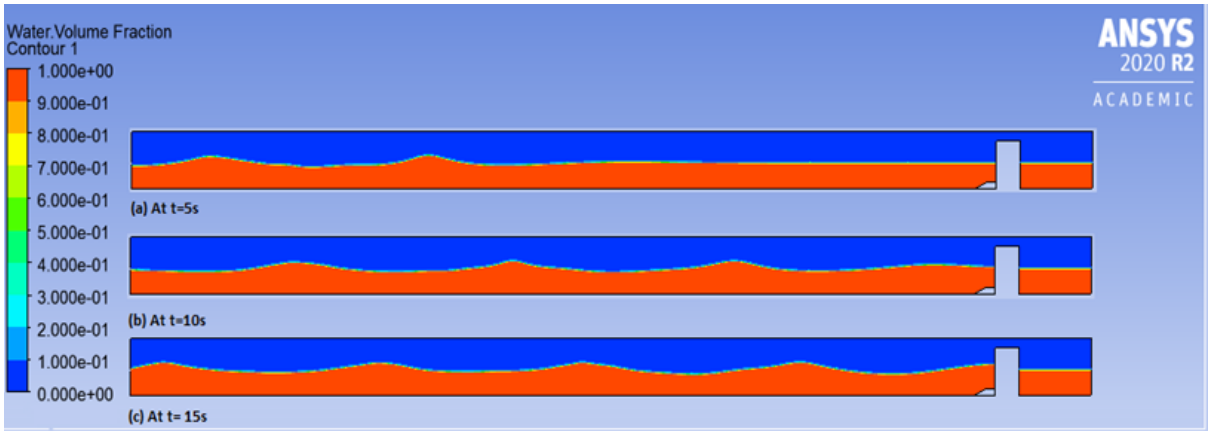

Figure 8: Propagation of waves in the numerical wave tank at an instant of time (a) 5 s, (b) 10 s, and (c) 15 s (at wave height of 0.12 m and a wave period of 2.2 s condition).

The pressure distribution (Fig 9) in the numerical wave flume has shown in Fig 9 at 6 s, 11.1 s & 12.2 s also strengthens the force on wall breakwater shown in Fig 6 (b). From Fig 9, the pressure on the lee side of the test model was not varied with time, indicating no transmission of energy from the lee side of the test model to the right side of the test model.

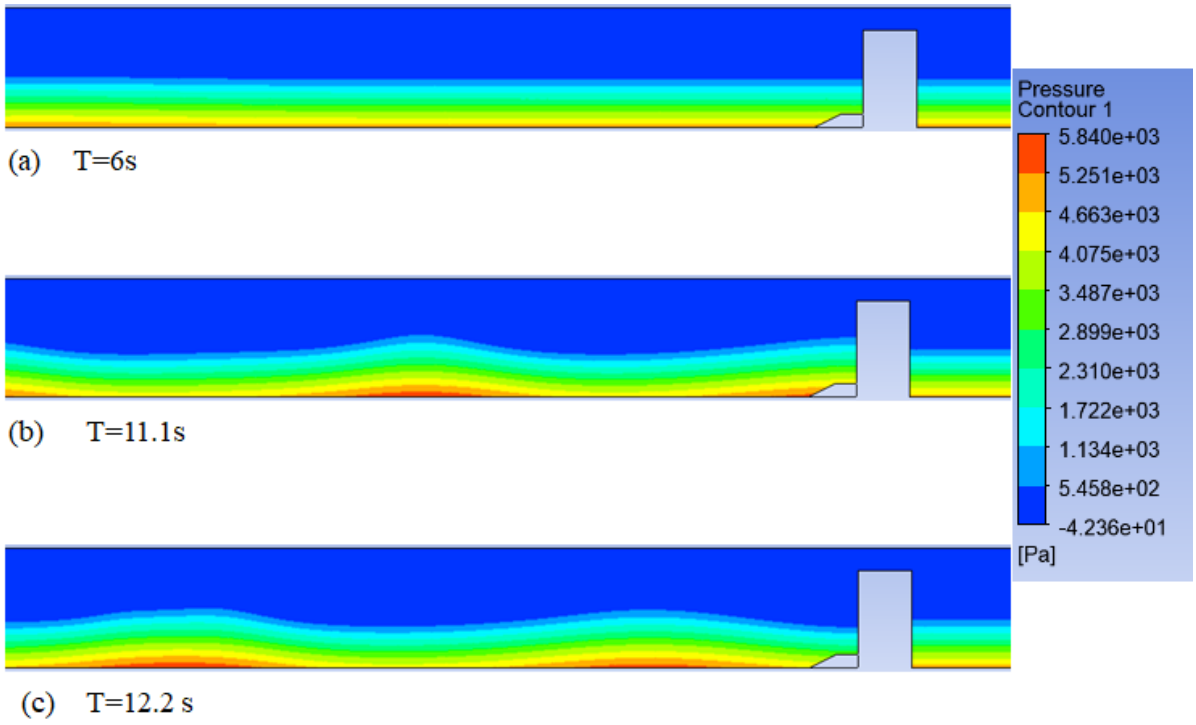

Figure 9: Pressure distribution in the numerical wave tank at (a) 6 s, (b) 11.1 s, and (c) 12.2 s (at wave height of 0.12 m and a wave period of 2.2 s condition).

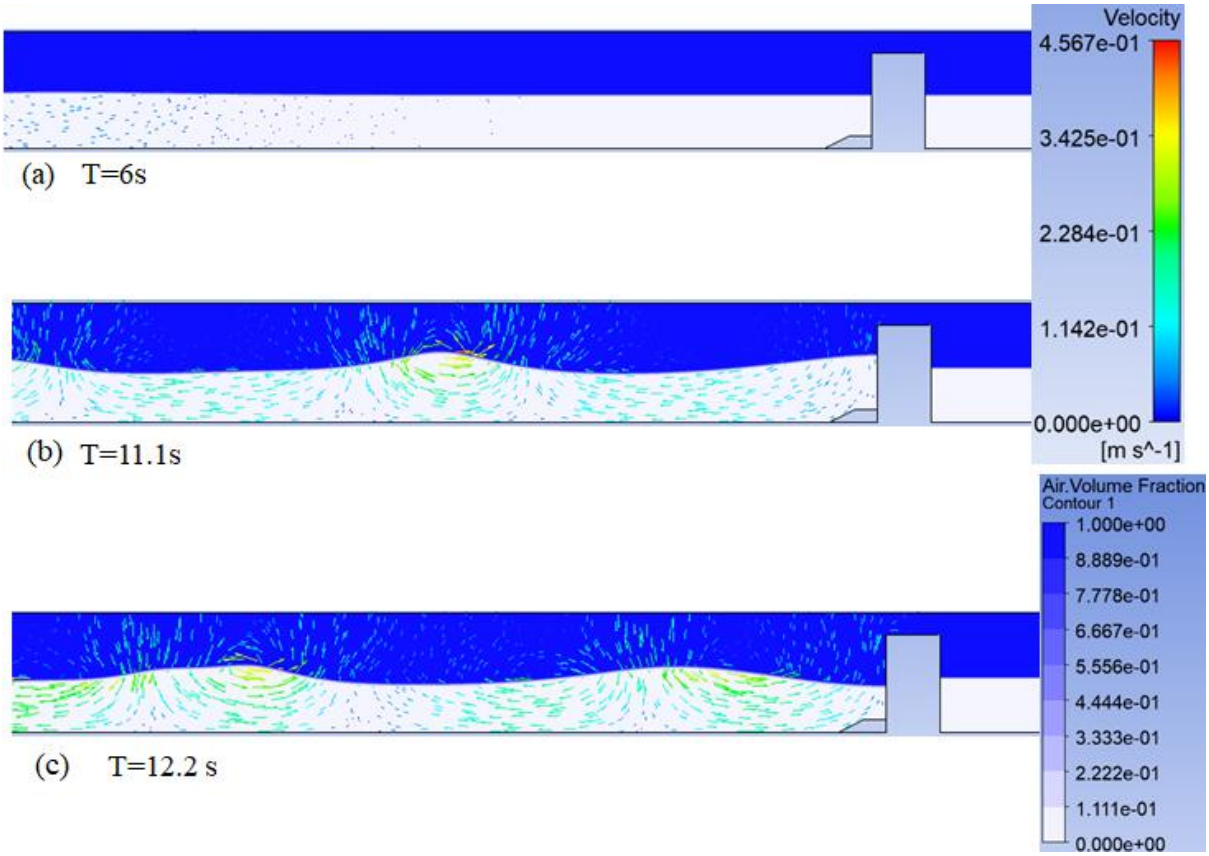

Figure 10: Magnitude and direction of fluid-particle (water and air) velocity in a numerical flume during propagation of wave under wave height of 0.12 m and a wave period of 2.2 s condition.

The velocity of water and air particles during wave structure interaction at a wave height of 0.12 m and a wave period of 2.2 s condition is shown in Figure 10. The velocity profiles are depicted along with the air volume fraction. The colour intensity of arrows indicates the magnitude of the velocity, and the direction of arrows shows the path of particle velocity. The motion of water particles is towards the test model before the wave starts interaction with the test model (Figure 10 (a)). The backflow of water particles from the test model is observed when the structure attained maximum run-up (Figure 10 (b)).

The velocity of water particles is more at 11.1 s more when compared to the velocity of water particles at 6 s, which increases the run-up on the test model and subsequently wave forces. Figure 10 (c) shows the fully developed wave to interact with the test model. The water particle velocities are maximum at a fully developed wave crust location. In the present study, at all experimental conditions, water depth is less than half of the wavelength, which implies the water particles move in an elliptical shape. Figure 10 is evident for the elliptical motion of water particles due to the interaction of the wave with the sea bed. Figure 9 is also evidence for an interaction of the wave with the sea bed, and the highest pressure on the sea bed is due to static and dynamic wave pressure.

5.1 Comparison of relative wave force ($P/\rho gd^2$) variation with wave steepness (H_i/L) on the wall for experimental, numerical, and theoretical approaches

Figure 11 illustrates the variation of relative wave force ($P/\rho gd^2$) with wave steepness (H_i/L) on the wall for the present experimental measured values. It is compared with the corresponding values calculated by theoretical formulae Goda and also by numerical approach. The wave force P is made non-dimensional by dividing over the term (ρgd^2) and plotted on the y-axis. The x-axis indicates the wave steepness (H_i/L). The dashed line, solid line, and dotted circle represent the theoretical, experimental, and numerical results, as shown in Figure 11. It is observed that the relative wave force is increasing with the increase in the wave periods and wave heights.

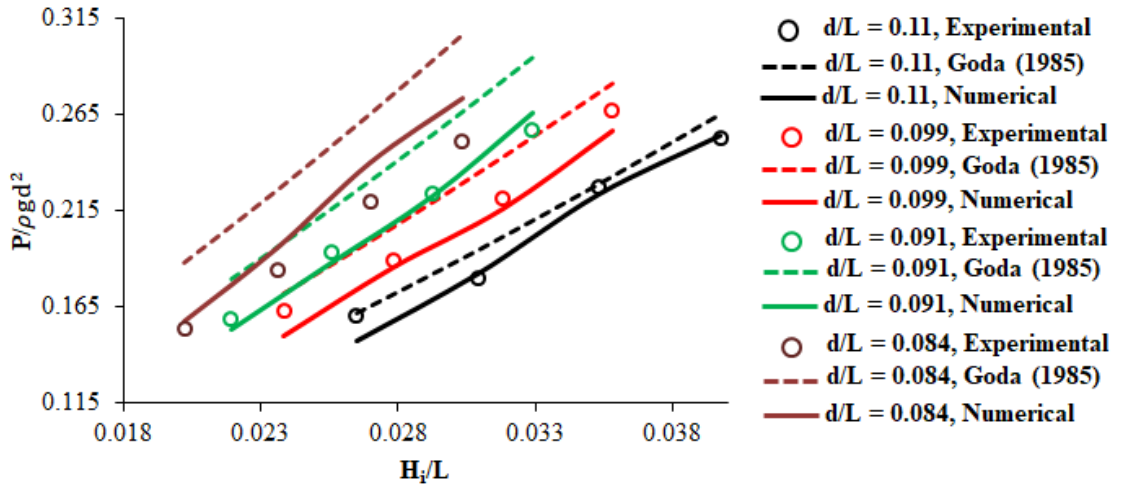

Figure 11: Variation of Wave force Parameter (F/ρgd2) with incident wave Steepness (Hi/L)

The wave force is calculated using Goda's theoretical approach, and it is observed that the relative wave force increases with the increase in the wave periods and wave heights. Since the long-period waves exert more pressure than short-period waves. Goda's method provides a reasonable estimation of wave force distribution which is comparable with the experimental results. This is due to that long period waves exert more force than short period waves (Yung-Fang Chiu 2007). The numerical results provide a reasonable estimation of wave force comparable with the experimental results for waves of small Ursell number. It is observed that the theoretical approach slightly overestimates the wave force for longer period waves.

5.2 Comparison of relative wave run-up (R_u/H_i) variation with relative water depth (d/L) on the wall for experimental and numerical approaches

The variation of relative wave run-up (R_u/H_i) as a function of relative water depth (d/L) is illustrated in Figure 12 for various relative wave heights (H_i/d). In general, the wave run-up is defined as the vertical rise of water above the still-water level to which the water rushes up on the front face of the test model. This helps in determining the design wave crest level of the structure depending on the allowable overtopping level.

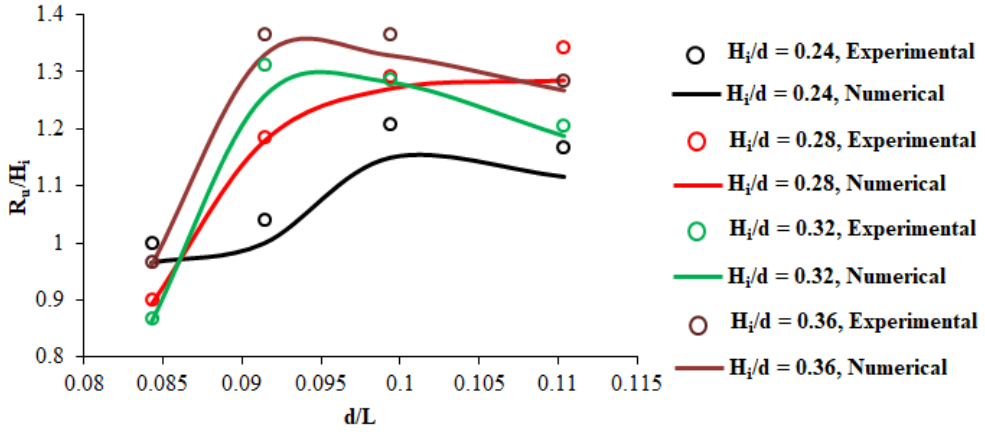

Figure 12: Variation of relative wave run-up (Ru/Hi) with relative depth parameter (d/L)

The relative run-up (R_u/H_i) decreases for an increase in the relative depth (d/L). The (R_u/H_i) increases with an increase in H_i/d because the higher wave heights rush up the waves above still water level. From the experimental results, the relative run-up (R_u/H_i) varies between 0.85 to 1.4.

5.3 Influence of wave steepness parameter (H_i/L) on wave reflection coefficient (K_r)

Figure 13 shows the effect of wave height on the coefficient of reflection K_r, in terms of wave steepness, H_i/L for different wave periods (d/L 0.084, 0.091, 0.099, and 0.11) on caisson breakwater. The wave surface elevation time histories from the wave probes are used to estimate the reflected wave heights (H_r). Three-wave probes are positioned at L (wavelength), L/3, and 2L/3 distance from the test model used to measure incident and reflected wave heights.

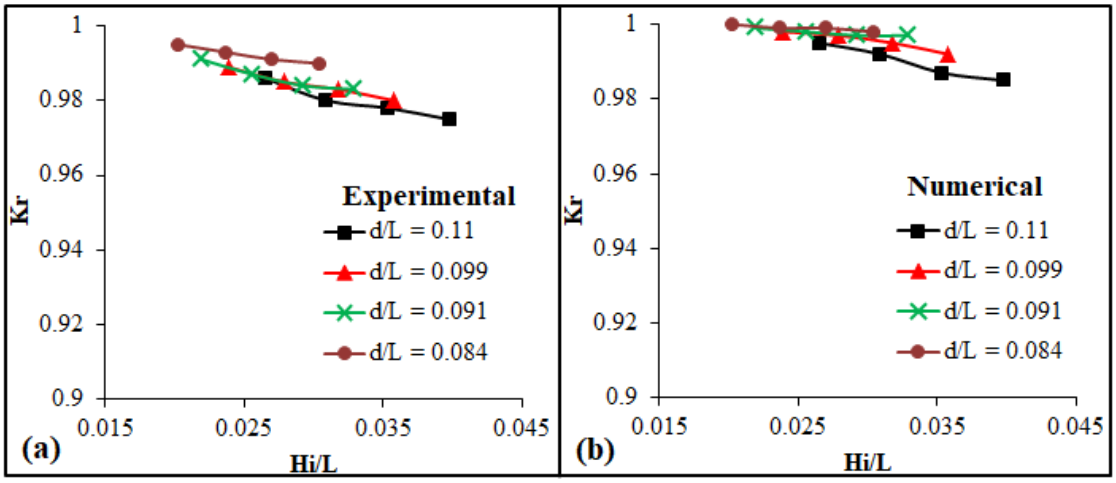

Figure 13: Variation of wave reflection coefficient (K_r) with wave steepness parameter (H_i/L)

The reflection coefficient K_r is obtained from the analysis of composite wave elevation using the transfer function method discussed by Shutang Zhu (1999). The reflection coefficient K_r is obtained from the study of composite wave elevation using the transfer function method discussed by Shutang Zhu (1999) and also calculated using MIKE Zero WS reflection analysis module, which is used for wave reflection analysis.

The governing equations using the least-squares fit approach are based on the method proposed by Mansard and Funke (1987) and extended by Zelt and Skjelbreia (1992). And also, the analysis requires measurements of waves at a minimum of two different locations are more to solve. The wave reflection coefficient (K_r) is defined as the square root of the ratio of the area between the reflected wave energy spectrums to the incident wave energy spectrum. From the observation, the reflection coefficient Kr is more than 0.97 for all the approaches.

5.4 Error Analysis

The results of the developed numerical wave flume and taking into consideration all parameters. It is concluded that simulations using mesh size 0.02, with a time step 0.01 s, 16 m flume length, provide the best solution, with an excellent agreement with experimental findings. Figure 14 represents the percentage of relative force error with wave heights. It can be seen that the error through all the domain lengths is minimal. For a particular wave period, the percentage of error increased with an increase in wave height.

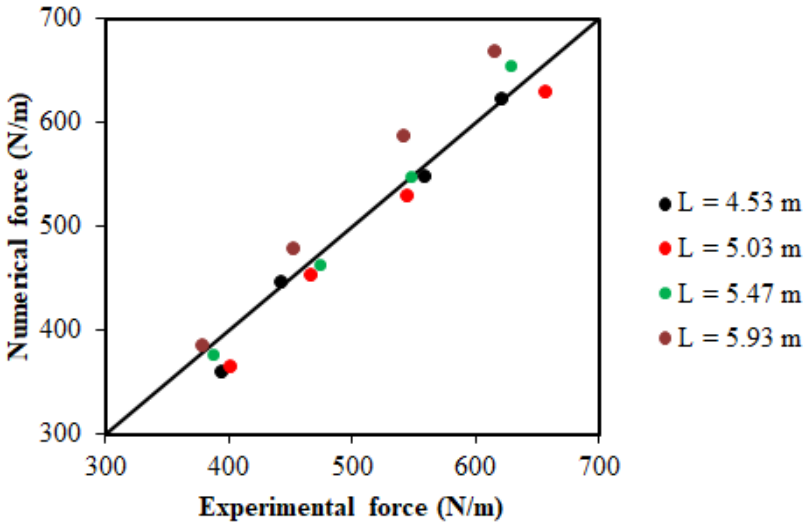

Figure 14: Error Analysis

The maximum percentage of error is observed at a wavelength of 5.93 m. The increases in the percentage of error with increases in wave height and wavelength are due to higher Ursell number, which influences the nonlinearity in the wave nature.

6. Conclusions

In this present study, an attempt is made to select the proper numerical model to study the hydrodynamic characteristics of the wall-type breakwater. The hydraulic performances of the wall-type breakwater are estimated using numerical modeling under different wave characteristics. The numerical results are validated using experimental findings, and the following conclusions are drawn.

- VOF model with a standard k-epsilon viscous model with Stokes third-order wave theory is appropriate to simulate the experimental conditions considered in this study, with a permissible error.
- The numerical model used in this study can estimate hydrodynamic characteristics of wall type-breakwater with less error at smaller wave height and wave periods. The error in estimated force on caisson breakwater is increased up to 6.8 % for wave height of 0.18 m conditions.

- The wave forces on vertical caisson type breakwater obtained from the numerical analysis showed a good correlation with experimental and theoretical (Goda, 1985) approaches.
- In numerical analysis, for shallow/intermediate wave conditions, the increase in wave height and wave period form unstable waves due to a rise in Ursell number, leading to increasing error in the estimated numerical results. At the same time, the grid resolution at specific regions of interest, different mesh sizes can be used in a computation simulation. This will result in more accurate and efficient computation.

Acknowledgment

The authors are thankful to the Director, NITK, Head, Dept. of Water Resources and Ocean Engineering for providing the Laboratory facilities and for their continuous support in conducting the experiments. The authors express gratitude to Central Research Facility, NITK for providing access to ANSYS software. We gratefully acknowledge the financial assistance provided by the Ministry of Earth Sciences under ESTC-COT cell, Govt. of India.

References

ANSYS, Inc. ANSYS FLUENT. Release 20.0: Theory guide.
Dentale, F., Reale, F., Di Leo, A., and Carratelli, E. P. (2018): A CFD approach to rubble mound breakwater design. Int. J. Nav. Archit. Ocean Eng., 10(5), 644–650.
Det Norske Veritas (2010): Environmental conditions and environmental loads, recommended practice. DNV-RP-C205, Oslo.
Du, Q., and Leung, D. Y. C. (2011): 2D Numerical Simulation of Ocean Waves, Proc. World Renew. Energy Congr., 57, 2183–2189.
Fábio, M., Marques, M., António, M., Gameiro, L., Almerindo, D., and Ferreira (2018): Numerical simulation of regular waves: Optimization of a numerical wave tank, Ocean Eng., 170, 89-99.
Gao, X. & Inouchi, K. (1998): The characteristics of scouring and depositing in front of vertical breakwaters by broken clapotis, Coastal Engineering Journal, 40:1, 99-113, https://dx.doi.org/10.1142/S0578563498000078
Goda, Y., and Suzuki, Y. (1976): Estimation of incident and reflected waves in random wave experiments. 15th International Conference on Coastal Engineering (ASCE), Honolulu, Hawaii.
Hajivalie, F., and Yeganeh-Bakhtiary, A. (2009): Numerical study of breakwater steepness effect on the hydrodynamics of standing waves and steady streaming. J. Coastal Res.
Hajivalie, F., Yeganeh-Bakhtiary, A., and Hashemi-Javan, A. (2010): Numerical simulation of wave breaking over a vertical breakwater. Int. J. Civ. Eng., IUST.
Hamza, S.B., Habli, S., Saïd, N.M., Bournot, H., and Le Palec, G. (2015): Numerical Simulation of Wave-Structure Interaction around an Obstacle, Design and Modeling of Mechanical Systems – II, Lecture Notes in Mechanical Engineering, Springer, Cham.
Hughes, S.A. (1993): Physical Models and Laboratory Techniques in Coastal Engineering. World Scientific, Hong Kong.
Kamath, A. M. (2012): Wave Forces on Structures Using Reef 3d., M.sc Thesis, NTNU.
Kasem, T., and Sasaki, J. (2011): Multiphase Modeling Of Wave Propagation Over Semicircular Obstacles Using Weno And Level Set Methods, Coastal Engineering Proceedings, 32, https://dx.doi.org/10.9753/icce.v32.waves.57.
Kumaran, V., Manu & Rao, S (2021). Damage Analysis of Toe for Wall Type Breakwaters. J. Inst. Eng. India Ser. A . https://dx.doi.org/10.1007/s40030-021-00591-4
Kumaran, V., Manu, Rao, S. (2021): Assessment of dynamic pressure and wave forces on vertical-caisson type breakwater Mar. Georesour. Geotechnology pp. 1-12
Mansard, E.P.D., and Funke, E.R. (1980): The measurement of incident and reflected spectra using a least squares method." Proc. 17th Coast. Eng. Conf., ASCE, 154–172.
MIKE Zero [Computer software]. Danish Hydraulic Institute, Hørsholm, Denmark.
Ning, D. Z., Wang, R. Q., Zou, Q. P., and Teng, B. (2016): An experimental investigation of hydrodynamics of a fixed OWC Wave Energy Converter., Appl. Energy., 168, 636–648.
Ning, D. Z., Wang, R. Q., Zou, Q. P., and Teng, B. (2016): An experimental investigation of hydrodynamics of a fixed OWC Wave Energy Converter., Appl. Energy., 168, 636–648.

Scarpetta, F., Gurnari, L., Torresi, M., Filianoti, P., and Camporeale, S. (2017): A CFD simulation of a full-scale U-OWC breakwater, Proceedings of the Twelfth European Wave and Tidal Energy Conference, 1014, 1-8.
Somervell, L.T., Thampi, S.G., and Shashikala, A.P. (2017): Hydrodynamic characteristics of the vertical cellular breakwater. J. Waterway, Port, Coast. Ocean Eng., 143(5): 04017015, https://dx.doi.org/10.1061/(ASCE)WW.1943-5460.0000404.
Poguluri, S. K. and Cho, I. H. (2020): Analytical and numerical study of wave interaction with a vertical slotted barrier, Ships and Offshore Structures, https://dx.doi.org/10.1080/17445302.2020.1790299.
Venkateswarlu, V, and Karmakar, D. (2020). Wave motion over stratified porous absorber combined with a seaward vertical barrier, Proceedings of the Institution of Mechanical Engineers, Part M: Journal of Engineering for the Maritime Environment, 234(4):830-845, https://dx.doi.org/10.1177/1475090220912643.
Vijay, K. G., and Sahoo, T. (2019): Scattering of Surface Gravity Waves by a Pair of Floating Porous Boxes." J. Offshore Mech. Arct. Eng., 141(5):051803. https://dx.doi.org/10.1115/1.4043415.
Wang, Y. X., Ren, X. Z., Dong, P., and Wang, G. Y. (2011): Three-dimensional numerical simulation of wave interaction with perforated quasi-ellipse caisson, Water Sci. Eng., 4(1), 46–60.
Xie, S. (1981): Scouring patterns in front of vertical breakwaters and their influences on the stability of the foundation of the breakwater, Report of Coastal Eng. Group, Delft, The Netherlands, 61.
Yeganeh-Bakhtiary, A., Houshangi, H., Hajivalie, F., and Abolfathi, S. (2017): A numerical study on hydrodynamics of standing waves in front of caisson breakwaters with WCSPH model, J. Coast. Eng., 59(1), 1–31.
Zelt, J. A., and Skjelbreia, J. E. (1992): Estimating incident and reflected wavefields using an arbitrary number of wave gauges. Proc., 23rd Int. Conf. on Coastal Engineering, https://doi.org/10.9753/icce.v2325p.
Zhao, L., and Liu, J. (2019): Three-dimensional numerical simulation of the interaction between regular waves and perforated caisson breakwater, International Society of Offshore and Polar Engineers.
Zhu, S. (1999): Separation of regular waves by a transfer function method, Ocean Eng.,26,1435–1446.